Tapping-mode SQUID-on-tip microscopy with proximity Josephson junctions

Rog, M.; Blom, T.J.; Boltje, D.B.; Haan, J.D. de; Fermin, R.; Niu, J.; ... ; Lahabi, K.

NANO LETTERS

pubs.acs.org/NanoLett
Letter

Tapping-Mode SQUID-on-Tip Microscopy with Proximity Josephson Junctions

Matthijs Rog, Tycho J. Blom, Daan B. Boltje, Jimi D. de Haan, Remko Fermin, Jiasen Niu, Yasmin C. Doedes, Milan P. Allan, and Kaveh Lahabi*

Cite This: Nano Lett. 2026, 26, 1608−1615

ABSTRACT: Studying nanoscale dynamics is essential for understanding quantum materials and advancing quantum-chip manufacturing. Still, it remains a major challenge to measure nonequilibrium properties such as current and dissipation, and their relationship to structure. Scanning nanoprobes utilizing superconducting quantum interference devices (SQUIDs) are uniquely suited here due to their unparalleled magnetic and thermal sensitivity. Here, we introduce tapping-mode SQUID-on-tip, which combines atomic force microscopy with nanoSQUID sensing. Our probes minimize the nanoSQUID−sample distance, provide in-plane magnetic sensitivity, and operate on realistic, highly corrugated nanostructures. Frequency multiplexing enables simultaneous imaging of currents, magnetism, dissipation, and topography. The large voltage output of our proximity-junction nanoSQUIDs allows us to resolve nanoscale currents as small as 100 nA using a simple four-probe electronic readout. By capturing local magnetic, thermal, and electronic response without external radiation, our technique offers a powerful noninvasive route to study dynamic phenomena in exotic materials and delicate quantum circuits.

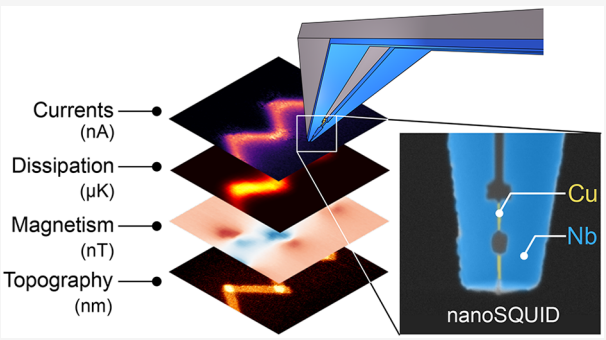

KEYWORDS: *SQUID, AFM, microscopy, Josephson effect, scanning*

Quantum materials stand out by their unusual nonequilibrium properties. From edge currents in topological devices to Planckian dissipation in strongly correlated matter, understanding the underlying physics requires local insights into the nature of transport and dissipation.[1−4] However, probing these quantities on the nanoscale is notoriously challenging. Moreover, in strongly interacting systems, it is well understood that transport and dissipation are closely interconnected with magnetism and system geometry. Due to the lack of a local probe to measure these fundamental quantities simultaneously, their local dynamics and interactions have remained elusive. Notable examples of this are phase transitions in many-body systems, where it is extremely challenging to identify the mechanism that triggers the transition.[5,6]

The need for such experimental probes is mirrored in the efforts toward working quantum computers. All superconducting and spin qubits are sensitive to local dynamics introduced by defects, such as magnetic impurities, vortices, and inhomogeneous supercurrents.[7−11] Identifying such sources of decoherence has been a major roadblock because their small experimental signatures can be detected only at cryogenic temperatures. In contrast, the techniques used for quantum-chip diagnostics are either cryogenically incompatible or suffer from insufficient sensitivity, poor spatial resolution, or invasive readout.

This work presents a microscope designed specifically to address these challenges. Our technique is capable of simultaneously recording magnetism, dissipation, charge transport, and topography on the nanoscale. Eliminating common sources of invasiveness, this microscope is innately compatible with fragile quantum systems. By recording in-plane magnetic fields with exceptionally sensitive sensors, this technique can resolve densely packed, complex current flow at the nanoscale with unprecedented detail and sensitivity. The incorporation of a robust topographic feedback mechanism makes the technique particularly suited for imaging complex nanodevices and quantum circuits that commonly exhibit substantial height variations. These four aspects of our technique open new possibilities in the research on quantum materials and devices inaccessible to established scanning probe techniques.

Received: September 10, 2025
Revised: November 27, 2025
Accepted: December 3, 2025
Published: January 27, 2026

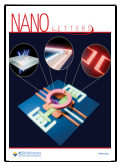

https://doi.org/10.1021/acs.nanolett.5c04571
Nano Lett. 2026, 26, 1608−1615

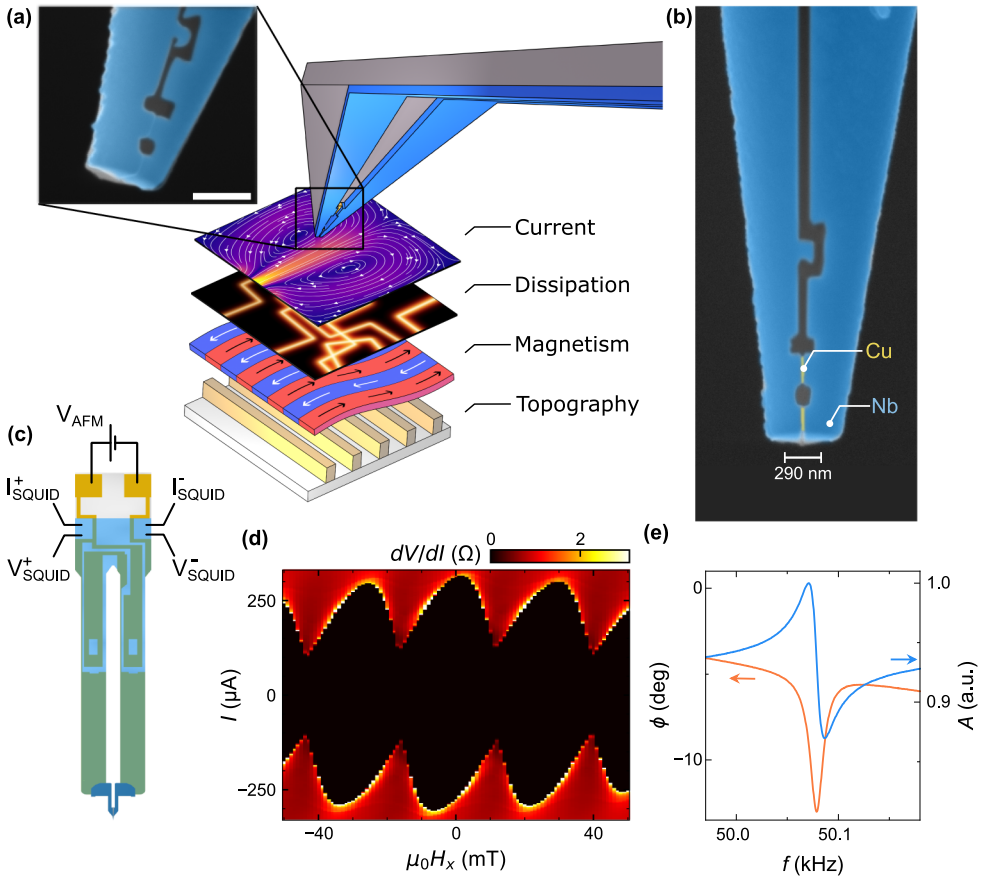

Figure 1. Overview of the tapping-mode SOT probe. (a) Schematic overview of the microscope. Our probes image the current, dissipation, magnetism, and topography simultaneously. The inset shows a scanning electron micrograph of a probe with a scale bar of 500 nm. (b) Scanning electron micrograph of a SOT probe, taken after 7 weeks of continuous usage. The effective diameter of the thin-film SQUID is 290 nm. (c) Overview of the quartz tuning fork. The SQUID devices are made on top of a commercial Akiyama tuning-fork AFM probe. The tuning-fork electrodes are shown in gold. Coverage of the SQUID thin films is shown in blue. (d) SQUID pattern of our device recorded at 2.5 K. (e) Resonance curve of the first cantilever bending mode recorded at 4 K. The data were recorded with a SQUID on the probe, illustrating that the presence of the SQUID does not modify the *Q* factor of the probe.

The integration of quantum sensors in scanning probe microscopy (SPM) has revolutionized our ability to study quantum phenomena on the nanoscale. For instance, scanning nitrogen-vacancy (NV) center microscopy has rapidly established itself as a standard technique capable of high-resolution imaging of magnetic phenomena and transport. At present, the sensitivity of this technique allows the mapping of small currents approaching 1 μA.[12] Although scanning NV was originally a room-temperature technique, much effort has gone into making it cryogenically compatible to study superconducting systems.[13−16] What is lacking are complementary cryogenic probes that have similar or better magnetic sensitivity, can measure local dissipation down to the microkelvin regime, and do not rely on invasive readout schemes that involve lasers and microwave radiation. Superconducting quantum interference devices (SQUIDs) stand out as ideal sensors to meet these requirements.

SQUIDs are the most sensitive electronic tools for measuring magnetic signals and are innately compatible with cryogenic temperatures. SQUID-based SPM techniques capitalize on this and have led to monumental breakthroughs in our understanding of quantum materials by probing exotic superconducting states,[18−20] phase transitions,[21,22] and quantum Hall states.[23] Of particular interest is SQUID-on-tip (SOT) microscopy, which unlocks exceptional spatial resolution by utilizing a nanoSQUID that directly scans the surface. This on-tip approach has enabled SOT to provide novel insights into vortex dynamics, topological matter, twisted bilayer graphene, and electron hydrodynamics.[24−29]

In addition to its exceptional magnetic sensitivity, SOT has a unique capacity for high-resolution thermal imaging at cryogenic temperatures. Its submicrokelvin thermal sensitivity surpasses that of other thermal microscopes by orders of magnitude, making it the only technique capable of mapping dissipation below the operation limit of a qubit.[30] Furthermore, SQUIDs utilize a fully electronic readout that does not rely on external radiation, making SOT noninvasive. The ability to probe local magnetism, dissipation, and transport, combined with its cryogenic operation, makes SOT ideal for studying fragile quantum systems.

Despite the great accomplishments of this microscope, there is opportunity for major advances that can realize the ultimate resolution and sensitivity of SOT and pave the way for it to become a mainstream SPM technique. Specifically, conventional SOT implementations lack the active height feedback required for robust topographic imaging and constant height control. As a result, SOTs typically scan at 100−250 nm above the surface, with flatter, crystalline samples allowing for closer approach.[28,31−33] Scanning too close to the surface greatly increases the risk of destroying the SQUID by crashing into

https://doi.org/10.1021/acs.nanolett.5c04571
Nano Lett. 2026, 26, 1608−1615

the sample. This restriction on the workable scan height not only reduces the measured signal but also sets the limit for spatial resolution. This issue is rooted in the design of existing SOT probes, where the SQUID is formed at the apex of a quartz tube.[34−36] Although the quartz tip is glued to a tuning fork, the tip−surface coupling is insufficient for stable topographic feedback.

A path to resolving this issue is to combine SOT with the powerful height control of atomic force microscopy (AFM). One implementation of this is SQUID-on-lever (SOL) microscopy, which fabricates the SQUID on a blunted AFM cantilever next to a small protruding tip.[37] Laser-based optical readout of the cantilever deflection enables simultaneous SQUID sensing and topographic imaging. SOL has been used to study magnetic ordering in 2D materials and magnetic inhomogeneities in spin qubits.[38,39] However, the sample−sensor distance in SOL implementations is generally limited to 100−300 nm by the protruding tip and the use of non-contact AFM. In a recent SOL design, the tip is omitted altogether and the nearby corner of the flat cantilever is used for height control, allowing a closer approach to a polished, crystalline sample surface.[40] More importantly, the laser used for the AFM readout can induce spurious interference in the sample, analogous to NV microscopy.[17] This undermines the non-invasive electronic readout of the SQUID. In general, the use of optical elements and the need for careful alignment complicates the integration of such microscopes in a cryogenic environment.

In this work, we present an SOT microscope that closes the SQUID-to-sample gap and provides robust topographic readout without relying on external radiation. Our probes operate fully electronically, without lasers, making them ideal for cryogenic operation. The unique design of our probe enables tapping-mode AFM, allowing us to scan nanofabricated devices with realistic topographic features. Even after weeks of continuous scanning in this mode, the probes showed no sign of degradation. Our probes are equipped with high-performance SQUIDs that utilize proximity Josephson junctions that have exceptionally large voltage output. This allows us to simplify the SQUID readout scheme to a four-wire measurement. Using these unique features, we resolve the distribution of nanoampere currents on the nanoscale in a densely packed nanostructure. The exceptional sensitivity of our SQUIDs, combined with the ability to image magnetism, transport, dissipation, and topography simultaneously, makes this technique a powerful tool to investigate quantum materials and devices.

We begin by highlighting the key characteristics of our probes. We fabricate our nanoSQUID at the apex of an AFM cantilever strongly coupled to a quartz tuning fork. An overview of the probe is presented in Figure 1a−c. Compared to traditional SOT and SOL probes, ours differ significantly in design and operation. The most apparent distinction is the orientation of the SQUID plane, which has a fixed 62° angle relative to that of the sample. By choosing this orientation, we allow the SQUID to probe both out-of-plane and in-plane components of the magnetic field. It also provides an additional degree of freedom to field-tune the SQUID, allowing us to maintain an optimal working point during field sweeps. This design is significantly more sensitive to in-plane magnetic signals, which enhances our capacity for spatially resolving small currents by decreasing the size of the point spread function (see the Supporting Information for further details).

We produce our sensors on top of commercial tuning-fork AFM sensors instead of standard cantilevers because tuning-fork sensors do not require optical readout. Specifically, we use Akiyama probes, which are both self-sensing and self-actuating, enabling fully electronic readout with only two wires.[41] In addition to being noninvasive, our fully electronic readout scheme is much simpler to implement in a cryostat because it avoids the need for optical access and alignment. A schematic of this probe is shown in Figure 1c. It operates by coupling the vibration of a piezoelectric tuning fork to a thin silicon cantilever mounted between its prongs. The resulting resonance modes can be used for topographic sensing. We employ the first cantilever bending mode, shown in Figure 1e, to perform both non-contact and tapping-mode AFM.[42] This mode keeps the tuning fork off-resonance and only resonates the cantilever, stabilizing the tapping mode.

Utilizing tapping-mode (also called dynamic-mode) AFM, we close the gap between the nanoSQUID and the surface. In this mode, the topographic feedback is determined by the repulsive part of the tip−sample interaction potential.[43] This ensures that the spatial resolution of the SOT is set only by the nanoSQUID size and oscillation amplitude.

A key feature of the nanoSQUID sensors in our probes is the use of proximity Josephson junctions with a normal metal barrier (SNS junctions), formed by an ∼20-nm-long copper nanobridge exposed through Ga^+ focused-ion-beam milling. The major advantage of using fully metallic proximity weak links, compared to other types of Josephson barriers, is their nonhysteretic current−voltage characteristics at all temperatures. In contrast, traditional SOT and SOL probes use Dayem (constriction) bridges, which are known to be hysteretic, especially far below the superconducting transition temperature.[44−46] In addition, our niobium−copper nanoSQUIDs have an exceptional transfer function of a few mV/Φ_0 (see the Supporting Information), which is at least 1 order of magnitude higher than the typical values reported for nanoSQUIDs.[47] The probe used to generate the figures in the main text realizes a field noise of 42 $nT/Hz^{1/2}$ and a temperature noise of 5.6 $\mu K/Hz^{1/2}$. Our junctions have a single-valued current phase relation at all temperatures and maintain their characteristics in the millikelvin regime.[48,49]

Utilizing multilayer heterostructures, we created a probe platform that enables flexible sensor customization. The versatility of the direct-write approach implemented here allows us to fabricate sensors ranging from 50 nm to several micrometers, depending on the desired trade-off between field sensitivity and resolution. The geometry of the device is easily modified, allowing us to tune the SQUID asymmetry and thus its zero-field sensitivity. This is of particular interest to the study of spontaneous time-reversal symmetry breaking and field-sensitive quantum devices.

The supercurrent interference pattern of a typical AFM−SQUID probe is shown in Figure 1d. The large gradient in differential resistance, the deep modulation of the pattern, and the substantial I_cR_N product all contribute to the exceptional transfer function of our nanoSQUIDs. Due to the resulting large voltage, cryogenic amplifiers are no longer strictly necessary. All of the measurements presented here were recorded in current-bias mode, using only a lock-in amplifier. This greatly simplifies our electronic setup and streamlines the operation of the microscope.

https://doi.org/10.1021/acs.nanolett.5c04571
Nano Lett. 2026, 26, 1608−1615

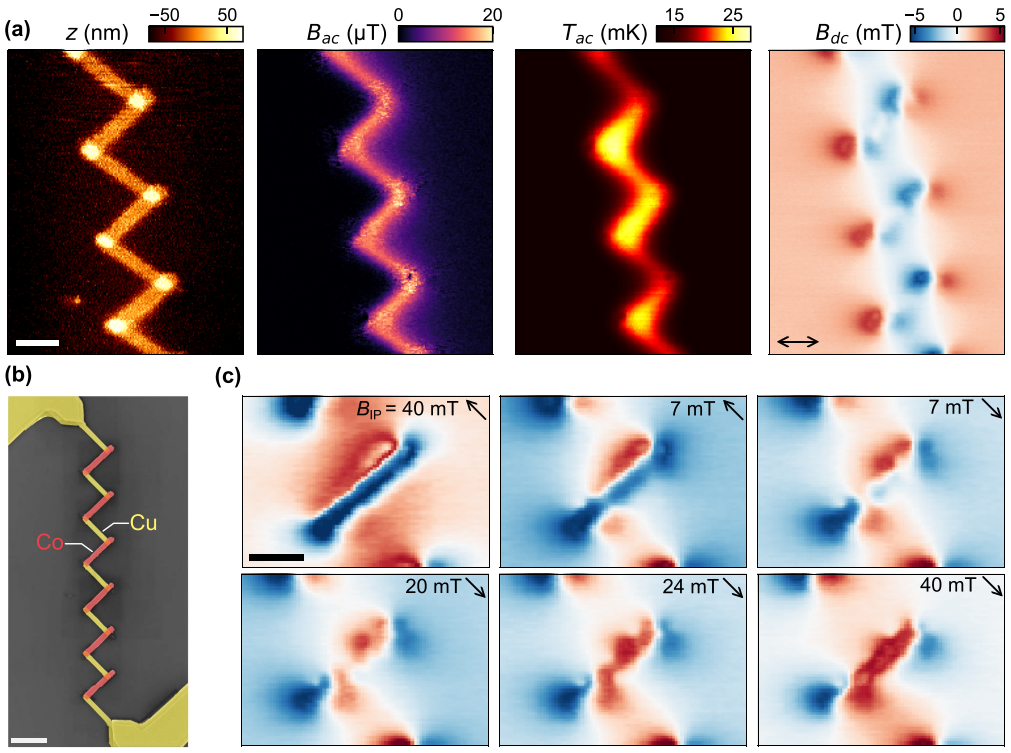

Figure 2. SOT images of a copper−cobalt heterostructure. (a) Simultaneously acquired images of topography, current, dissipation, and magnetism, while exciting the heterostructure with an ac current of 100 μA rms. The scale bar denotes 2 μm. The arrow in the rightmost panel denotes the (sensitive) SQUID axis. (b) Scanning electron micrograph of the sample. The scale bar denotes 5 μm. (c) Single cobalt micromagnet in various perpendicular fields highlighting domain-wall formation. The arrow in the panel denotes the in-plane field size and direction. Using our vector magnet, we simultaneously apply out-of-plane fields between −40 and +40 mT so that the probe remains at its most sensitive point during every scan. The scale bar denotes 2 μm. The total range of all images is 8 mT.

The experiments were performed inside a continuous-flow cryostat with its pulse tube running. We observed no interference from the pulse tube in our experiments. Even after 7 weeks of continuous imaging in tapping mode, neither the probe nor the sample showed any signs of degradation.

We demonstrate the working principle of the microscope with a magnetic heterostructure consisting of alternating cobalt and copper nanowires, shown in Figure 2b. Due to the shape anisotropy, the cobalt is naturally magnetized along its long axis, creating dipole fields that can be imaged with our SQUID. Applying a current through the sample generates magnetic fields as well as dissipation from Joule heating.

Using an alternating-current (ac) bias, we demonstrate simultaneous imaging of all relevant parameters. The current generates magnetic fields at a frequency f, while the Joule heating oscillates at $2f$. The dipole fields are static and can therefore be measured via the SQUID's direct-current (dc) voltage. This frequency multiplexing method was first used by Halbertal et al.[30]

We simultaneously record the topography, static magnetic fields, current-induced ac fields, and resulting heat, as shown in Figure 2a. Although the ac and dc signals differ by more than 2 orders of magnitude, the frequency-separation technique provides images that are nearly completely artifact-free. We obtained quantitative measurements using a simple one-to-one calibration (see the Supporting Information). Comparing this with the topographic image, we see that both transport signals are confined to the nanowire, underscoring the probe's utility as a local current sensor. The thermal image shows a contrast between cobalt and copper segments due to their resistivity mismatch. The increased dissipation at the wire ends may indicate finite interface resistance.

Because our SQUIDs respond to both in-plane and out-of-plane fields, they can be used at their optimal sensitivity over a large and continuous range of background fields. We illustrate this with an experiment in Figure 2c, where we image the magnetization reversal of the cobalt wires while sweeping an in-plane field. Initially, we magnetized the cobalt wires by applying a 200 mT field along their short axis, which is then incrementally inverted. We image the capture and gradual propagation of a domain wall, leading to a magnetization reversal in the bar. Because the magnetization of cobalt nanostructures is insensitive to small out-of-plane fields, we use an out-of-plane field to keep the SQUID at its working point at all times. This additional degree of freedom is available because of the 62° angle between the SQUID and the surface.

We proceed by benchmarking the unique capabilities of the microscope as a local probe for high-resolution transport phenomena. To characterize its current imaging capacity, we study a high-density niobium serpentine nanostructure, as shown in Figure 3a.

In Figure 3b, we present a magnetic image of the serpentine driven by an ac current of 100 μA rms. Our in-plane sensitivity reveals the local current distribution, including clear sign inversions where the current reverses direction. This level of detail is inaccessible using conventional out-of-plane techniques.

We assess the probe's sensitivity by performing line scans at various applied currents. Figure 3c shows the raw signals at 10 and 1 μA without any integration or postprocessing. Both

https://doi.org/10.1021/acs.nanolett.5c04571
Nano Lett. 2026, 26, 1608−1615

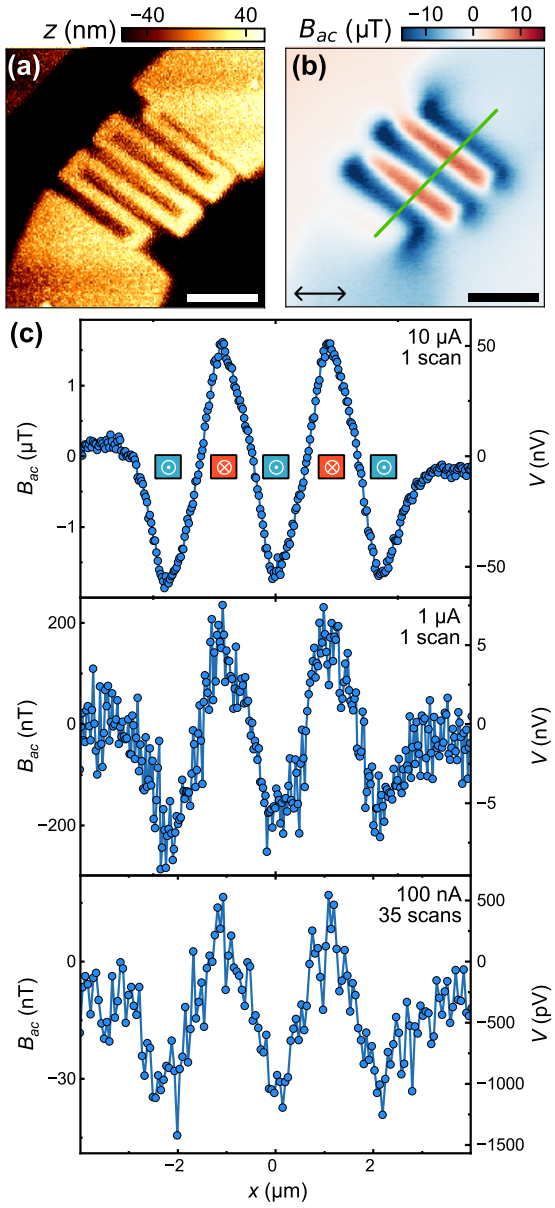

Figure 3. Nanoresolved imaging of small supercurrents. (a) Topographic image of the niobium serpentine. (b) Magnetic field generated by a 100 μA current. The arrow indicates the SQUID axis. (c) Line scans taken along the green line in part b, each taken at a different excitation current, using lock-in time constants of 100, 150, and 750 ms. The drawing in the top panel shows the position of the wires and current direction. All scale bars: 2 μm.

signals exhibit a good signal-to-noise ratio (SNR) and low field noise.

Subsequently, we demonstrate the probe's ability to resolve submicroampere currents by reducing the current to 100 nA. Our ability to simultaneously record topography is vital here because it allows pixel-perfect alignment of multiple line scans, which can be integrated to obtain a high-SNR trace. This represents a significant improvement over previous out-of-plane imaging works, none of which could reach such low currents at submicron spatial resolution.[36,50−52]

We now describe how our technique can also be applied to static fields such as those generated by magnetic materials and spontaneous supercurrents. The detection of small currents is typically done using ac techniques, to avoid $1/f$ noise, but these methods are not applicable to static fields. In our microscope, we address this problem by lightly oscillating the sample in the out-of-plane direction, thereby converting static signals to an ac flux. Similar methods were previously used in scanning NV,[53] SOT,[31] and SOL.[37]

Using this gradiometric imaging, we investigate the supercurrents flowing around Pearl vortices, which are the thin-film counterparts of Abrikosov vortices. In Pearl vortices, the supercurrent is expected to decay over the Pearl length $\Lambda = 2\lambda^2/d$, where λ is the London penetration depth and d is the film thickness.

In Figure 4a,b, we show images of randomly distributed vortices in a 0.1 mT field-cooled, 60-nm-thick niobium film (T_c = 8.8 K). This arrangement of vortices is a product of the large intervortex spacing and the natural pinning sites present in the film. In this case, pinning forces dominate vortex−vortex repulsion, preventing the formation of an Abrikosov lattice.

Due to our large in-plane sensitivity, the vortex images look different from most conventional imaging techniques. To illustrate this point, Figure 4c shows the field for a single vortex, using the SQUID height and a representative Pearl length for the measurement in Figure 4b. The fields extend far beyond the core, tracing the rotating supercurrent around the vortex. Because the probe measures both in-plane and out-of-plane field components, there is an offset between the symmetry point of the field pattern and the vortex core. Compared to theory, the experimental data show a slight elongation due to piezo nonlinearity.

Next, we study vortices in confined geometries: a triangle, a circle, and a square microstructured from a 70 nm niobium film. We cool the structures below the transition temperature while applying small out-of-plane fields, ranging from 0.6 to 1.2 mT, and image the emerging vortices.

At 0.6 mT, a single vortex is present in the circle and two vortices are present in the square. In the triangle, however, a vortex appears only when 1.2 mT is applied. At this field, the circle and square host three and four vortices, respectively. We emphasize that the system is fully deterministic: experiments can be repeated over multiple thermal cycles, and fields below 0.2 mT result in a vortex-free state.

The differences in the nucleation fields can be understood through the potential energy landscapes of the three geometries. In thin-film nanostructures, vortex entry is governed by the Gibbs free energy, where the kinetic energy of the vortices competes against the vortex−Meissner repulsion. This interaction pushes vortices away from the edges and toward the center of a microstructure.[54] Because the triangle has a larger perimeter-to-area ratio, it has the highest Gibbs barrier and requires a higher field for the first vortex to enter. Note that when the first vortex enters the triangle at 1.2 mT, the enclosed flux is already 7.2 Φ_0. In contrast, in the circle, the first vortex enters at 4.9 Φ_0 and the square hosts two vortices at 6.0 Φ_0.

In summary, we have introduced tapping-mode SOT, which utilizes a noninvasive electronic readout to simultaneously probe topography, magnetism, transport, and dissipation. We benchmarked the microscope in magnetic hybrids and superconducting devices, where we demonstrate how in-plane field sensitivity and the large transfer function of the proximity nanoSQUID enable us to resolve currents down to 100 nA. The ultrahigh sensitivity of our probes to magnetic, thermal, and transport phenomena makes this an ideal

https://doi.org/10.1021/acs.nanolett.5c04571
Nano Lett. 2026, 26, 1608−1615

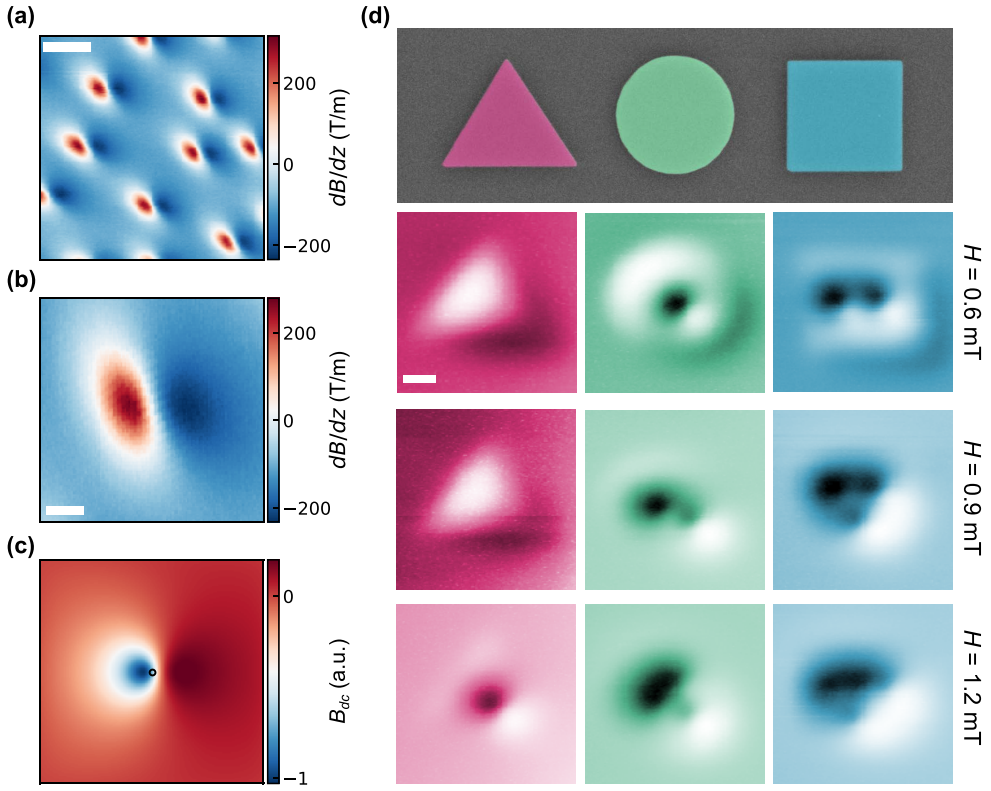

Figure 4. Vortex imaging performed with our SOT in its gradiometric imaging mode, where the sample is oscillated out-of-plane with 35 nm rms. Instead of imaging the vortex core, we observe the currents flowing around it. (a and b) Pearl vortices in an niobium thin film. These images are taken in noncontact AFM mode at a constant height of 250 nm. Part b shows a close-up of a single vortex in the same thin film with a scale bar of 1 μm. (c) Simulated field of a single vortex for Λ = 570 nm, which corresponds to the expected Pearl length of our film at 3.1 K. The black circle marks the vortex core. The image size is the same as that of the image in part b. (d) Imaging vortices in microstructures using tapping-mode gradiometry. The top image shows a scanning electron micrograph of a triangle (side length of 5.3 μm), a circle (diameter of 4.6 μm), and a square (side length of 4.5 μm). These are cooled in a finite field, denoted to the right of the images. Various fields yield different vorticities depending on the edge-to-surface ratio. The scales of the images are, from top to bottom, for the triangles 500, 300, and 800 T/m, for the circles 750, 1400, and 1800 T/m, and for the squares 1000, 1400, and 2100 T/m. The scale bar in part a is 4 μm, and that in parts b–d is 1 μm.

technique for studying a wide range of quantum systems in both exotic matter and sensitive quantum devices.

■ ASSOCIATED CONTENT

Supporting Information

The Supporting Information is available free of charge at https://pubs.acs.org/doi/10.1021/acs.nanolett.5c04571.

Simulations of the role of SQUID orientation, details on the probe fabrication and properties, image calibration methods, and sample fabrication details (PDF)

■ AUTHOR INFORMATION

Corresponding Author

Kaveh Lahabi − *Huygens-Kamerlingh Onnes Laboratory, Leiden University, 2300 RA Leiden, The Netherlands; QuantaMap BV, 2333 CG Leiden, The Netherlands;* orcid.org/0000-0001-8070-7310; Email: lahabi@physics.leidenuniv.nl

Authors

Matthijs Rog − *Huygens-Kamerlingh Onnes Laboratory, Leiden University, 2300 RA Leiden, The Netherlands*

Tycho J. Blom − *Huygens-Kamerlingh Onnes Laboratory, Leiden University, 2300 RA Leiden, The Netherlands*

Daan B. Boltje − *QuantaMap BV, 2333 CG Leiden, The Netherlands*

Jimi D. de Haan − *QuantaMap BV, 2333 CG Leiden, The Netherlands*

Remko Fermin − *Huygens-Kamerlingh Onnes Laboratory, Leiden University, 2300 RA Leiden, The Netherlands; Department of Materials Science and Metallurgy, University of Cambridge, Cambridge CB3 0FS, United Kingdom*

Jiasen Niu − *Huygens-Kamerlingh Onnes Laboratory, Leiden University, 2300 RA Leiden, The Netherlands; Faculty of Physics and Munich Center for Quantum Science and Technology, Ludwig-Maximilians-University Munich, Munich 80799, Germany*

Yasmin C. Doedes − *Huygens-Kamerlingh Onnes Laboratory, Leiden University, 2300 RA Leiden, The Netherlands*

Milan P. Allan − *Huygens-Kamerlingh Onnes Laboratory, Leiden University, 2300 RA Leiden, The Netherlands; QuantaMap BV, 2333 CG Leiden, The Netherlands; Faculty of Physics, Center for Nano Science, and Munich Center for Quantum Science and Technology, Ludwig-Maximilians-University Munich, Munich 80799, Germany*

Complete contact information is available at: https://pubs.acs.org/10.1021/acs.nanolett.5c04571

https://doi.org/10.1021/acs.nanolett.5c04571
Nano Lett. 2026, 26, 1608−1615

Notes

The authors declare the following competing financial interest(s): K.L., M.P.A., D.B.B., and J.D.d.H. are, have been, or may in the future be participants in incentive stock plans at QuantaMap BV. The remaining authors declare no other competing interests.

■ ACKNOWLEDGMENTS

The authors thank Dalal Benali, Christiaan Pen, Peter van Veldhuizen, Fabian Steinmeyer, Maurits Geenen, and Luc Wigbout for their technical contributions and Johannes Jobst for helpful discussions. This work was financed by the Dutch National Growth Fund, as part of the Quantum Delta NL Programme in Project SME_R027_MQC, and the Dutch Research Council, as part of the "The Full Picture: Novel Microscopy with Smart Quantum Probes" (Project VI.Veni.212.302), "Three seeds for the quantum/nano-revolution" (Project NWA 1418.22.001), and Take-off Phase 2 (Project 20964). It was also partly supported by European Union via the NextGenerationEU program.

■ REFERENCES

(1) Hartnoll, S. A.; Mackenzie, A. P. *Colloquium*: Planckian Dissipation in Metals. *Rev. Mod. Phys.* **2022**, *94* (4), 041002.
(2) Keimer, B.; Kivelson, S. A.; Norman, M. R.; Uchida, S.; Zaanen, J. From Quantum Matter to High-Temperature Superconductivity in Copper Oxides. *Nature* **2015**, *518* (7538), 179−186.
(3) Bernevig, B. A.; Felser, C.; Beidenkopf, H. Progress and Prospects in Magnetic Topological Materials. *Nature* **2022**, *603* (7899), 41−51.
(4) Basov, D. N.; Averitt, R. D.; Van Der Marel, D.; Dressel, M.; Haule, K. Electrodynamics of Correlated Electron Materials. *Rev. Mod. Phys.* **2011**, *83* (2), 471−541.
(5) Avallone, G.; Fermin, R.; Lahabi, K.; Granata, V.; Fittipaldi, R.; Cirillo, C.; Attanasio, C.; Vecchione, A.; Aarts, J. Universal Size-Dependent Nonlinear Charge Transport in Single Crystals of the Mott Insulator Ca2RuO4. *Npj Quantum Mater.* **2021**, *6* (1), 91.
(6) O'Mahony, S. M.; Ren, W.; Chen, W.; Chong, Y. X.; Liu, X.; Eisaki, H.; Uchida, S.; Hamidian, M. H.; Davis, J. C. S. On the Electron Pairing Mechanism of Copper-Oxide High Temperature Superconductivity. *Proc. Natl. Acad. Sci. U. S. A.* **2022**, *119* (37). DOI: 10.1073/pnas.2207449119.
(7) Krantz, P.; Kjaergaard, M.; Yan, F.; Orlando, T. P.; Gustavsson, S.; Oliver, W. D. A Quantum Engineer's Guide to Superconducting Qubits. *Appl. Phys. Rev.* **2019**, *6* (2), 021318.
(8) Kim, R. H. J.; Park, J. M.; Haeuser, S.; Huang, C.; Cheng, D.; Koschny, T.; Oh, J.; Kopas, C.; Cansizoglu, H.; Yadavalli, K.; Mutus, J.; Zhou, L.; Luo, L.; Kramer, M. J.; Wang, J. Visualizing Heterogeneous Dipole Fields by Terahertz Light Coupling in Individual Nano-Junctions. *Commun. Phys.* **2023**, *6* (1), 147.
(9) Bilmes, A.; Megrant, A.; Klimov, P.; Weiss, G.; Martinis, J. M.; Ustinov, A. V.; Lisenfeld, J. Resolving the Positions of Defects in Superconducting Quantum Bits. *Sci. Rep.* **2020**, *10* (1), 3090.
(10) Bilmes, A.; Volosheniuk, S.; Ustinov, A. V.; Lisenfeld, J. Probing Defect Densities at the Edges and inside Josephson Junctions of Superconducting Qubits. *Npj Quantum Inf.* **2022**, *8* (1), 24.
(11) Altoé, M. V. P.; Banerjee, A.; Berk, C.; Hajr, A.; Schwartzberg, A.; Song, C.; Alghadeer, M.; Aloni, S.; Elowson, M. J.; Kreikebaum, J. M.; Wong, E. K.; Griffin, S. M.; Rao, S.; Weber-Bargioni, A.; Minor, A. M.; Santiago, D. I.; Cabrini, S.; Siddiqi, I.; Ogletree, D. F. Localization and Mitigation of Loss in Niobium Superconducting Circuits. *PRX Quantum* **2022**, *3* (2), 020312.
(12) Chang, K.; Eichler, A.; Rhensius, J.; Lorenzelli, L.; Degen, C. L. Nanoscale Imaging of Current Density with a Single-Spin Magnetometer. *Nano Lett.* **2017**, *17* (4), 2367−2373.
(13) Thiel, L.; Rohner, D.; Ganzhorn, M.; Appel, P.; Neu, E.; M üller, B.; Kleiner, R.; Koelle, D.; Maletinsky, P. Quantitative Nanoscale Vortex-Imaging Using a Cryogenic Quantum Magnetometer. *Nat. Nanotechnol.* **2016**, *11* (8), 677−681.
(14) Chen, S.; Park, S.; Vool, U.; Maksimovic, N.; Broadway, D. A.; Flaks, M.; Zhou, T. X.; Maletinsky, P.; Stern, A.; Halperin, B. I.; Yacoby, A. Current Induced Hidden States in Josephson Junctions. *Nat. Commun.* **2024**, *15* (1), 8059.
(15) Borst, M.; Vree, P. H.; Lowther, A.; Teepe, A.; Kurdi, S.; Bertelli, I.; Simon, B. G.; Blanter, Y. M.; Van Der Sar, T. Observation and Control of Hybrid Spin-Wave-Meissner-Current Transport Modes. *Science* **2023**, *382* (6669), 430−434.
(16) Jayaram, S.; Lenger, M.; Zhao, D.; Pupim, L.; Taniguchi, T.; Watanabe, K.; Peng, R.; Scheffler, M.; Stöhr, R.; Scheurer, M. S.; Smet, J.; Wrachtrup, J. Probing Vortex Dynamics in 2D Superconductors with Scanning Quantum Microscope. *Phys. Rev. Lett.* **2025**, *135*. DOI: 10.1103/1fzm-pb1d.
(17) Lillie, S. E.; Broadway, D. A.; Dontschuk, N.; Scholten, S. C.; Johnson, B. C.; Wolf, S.; Rachel, S.; Hollenberg, L. C. L.; Tetienne, J.-P. Laser Modulation of Superconductivity in a Cryogenic Wide-Field Nitrogen-Vacancy Microscope. *Nano Lett.* **2020**, *20* (3), 1855−1861.
(18) Tsuei, C. C.; Kirtley, J. R.; Chi, C. C.; Yu-Jahnes, L. S.; Gupta, A.; Shaw, T.; Sun, J. Z.; Ketchen, M. B. Pairing Symmetry and Flux Quantization in a Tricrystal Superconducting Ring of Y Ba 2 Cu 3 O 7 - δ. *Phys. Rev. Lett.* **1994**, *73* (4), 593−596.
(19) Kirtley, J. R.; Tsuei, C. C.; Ariando; Verwijs, C. J. M.; Harkema, S.; Hilgenkamp, H. Angle-Resolved Phase-Sensitive Determination of the in-Plane Gap Symmetry in YBa2Cu3O7-δ. *Nat. Phys.* **2006**, *2* (3), 190−194.
(20) Bert, J. A.; Kalisky, B.; Bell, C.; Kim, M.; Hikita, Y.; Hwang, H. Y.; Moler, K. A. Direct Imaging of the Coexistence of Ferromagnetism and Superconductivity at the LaAlO3/SrTiO3 Interface. *Nat. Phys.* **2011**, *7* (10), 767−771.
(21) Kremen, A.; Khan, H.; Loh, Y. L.; Baturina, T. I.; Trivedi, N.; Frydman, A.; Kalisky, B. Imaging Quantum Fluctuations near Criticality. *Nat. Phys.* **2018**, *14* (12), 1205−1210.
(22) Devidas, T. R.; Yahav, D.; Reichanadter, J. T.; Sterenberg, M.; Moore, J. E.; Neaton, J. B.; Analytis, J. G.; Kalisky, B. Dark Metastable Conduction Channels near a Metal-Insulator Transition. *arXiv* **2025**. DOI: 10.48550/arXiv.2405.02036.
(23) Ferguson, G. M.; Xiao, R.; Richardella, A. R.; Low, D.; Samarth, N.; Nowack, K. C. Direct Visualization of Electronic Transport in a Quantum Anomalous Hall Insulator. *Nat. Mater.* **2023**, *22* (9), 1100−1105.
(24) Embon, L.; Anahory, Y.; Jelić, Ž. L.; Lachman, E. O.; Myasoedov, Y.; Huber, M. E.; Mikitik, G. P.; Silhanek, A. V.; Milošević, M. V.; Gurevich, A.; Zeldov, E. Imaging of Super-Fast Dynamics and Flow Instabilities of Superconducting Vortices. *Nat. Commun.* **2017**, *8* (1), 85.
(25) Lachman, E. O.; Mogi, M.; Sarkar, J.; Uri, A.; Bagani, K.; Anahory, Y.; Myasoedov, Y.; Huber, M. E.; Tsukazaki, A.; Kawasaki, M.; Tokura, Y.; Zeldov, E. Observation of Superparamagnetism in Coexistence with Quantum Anomalous Hall C = ± 1 and C = 0 Chern States. *Npj Quantum Mater.* **2017**, *2* (1), 70.
(26) Tschirhart, C. L.; Serlin, M.; Polshyn, H.; Shragai, A.; Xia, Z.; Zhu, J.; Zhang, Y.; Watanabe, K.; Taniguchi, T.; Huber, M. E.; Young, A. F. Imaging Orbital Ferromagnetism in a Moiré Chern Insulator. *Science* **2021**, *372* (6548), 1323−1327.
(27) Tschirhart, C. L.; Redekop, E.; Li, L.; Li, T.; Jiang, S.; Arp, T.; Sheekey, O.; Taniguchi, T.; Watanabe, K.; Huber, M. E.; Mak, K. F.; Shan, J.; Young, A. F. Intrinsic Spin Hall Torque in a Moiré Chern Magnet. *Nat. Phys.* **2023**, *19* (6), 807−813.
(28) Grover, S.; Bocarsly, M.; Uri, A.; Stepanov, P.; Di Battista, G.; Roy, I.; Xiao, J.; Meltzer, A. Y.; Myasoedov, Y.; Pareek, K.; Watanabe, K.; Taniguchi, T.; Yan, B.; Stern, A.; Berg, E.; Efetov, D. K.; Zeldov, E. Chern Mosaic and Berry-Curvature Magnetism in Magic-Angle Graphene. *Nat. Phys.* **2022**, *18* (8), 885−892.
(29) Aharon-Steinberg, A.; Völkl, T.; Kaplan, A.; Pariari, A. K.; Roy, I.; Holder, T.; Wolf, Y.; Meltzer, A. Y.; Myasoedov, Y.; Huber, M. E.;

Yan, B.; Falkovich, G.; Levitov, L. S.; Hücker, M.; Zeldov, E. Direct Observation of Vortices in an Electron Fluid. *Nature* **2022**, *607* (7917), 74−80.
(30) Halbertal, D.; Cuppens, J.; Shalom, M. B.; Embon, L.; Shadmi, N.; Anahory, Y.; Naren, H. R.; Sarkar, J.; Uri, A.; Ronen, Y.; Myasoedov, Y.; Levitov, L. S.; Joselevich, E.; Geim, A. K.; Zeldov, E. Nanoscale Thermal Imaging of Dissipation in Quantum Systems. *Nature* **2016**, *539* (7629), 407−410.
(31) Fridman, N.; Feld, T. D.; Noah, A.; Zalic, A.; Markman, M.; Devidas, T. R.; Zur, Y.; Grynszpan, E.; Gutfreund, A.; Keren, I.; Vakahi, A.; Remennik, S.; Watanabe, K.; Taniguchi, T.; Huber, M. E.; Aleiner, I.; Steinberg, H.; Agam, O.; Anahory, Y. Anomalous Thickness Dependence of the Vortex Pearl Length in Few-Layer $NbSe_2$. *Nat. Commun.* **2025**, *16* (1). DOI: 10.1038/s41467-025-57817-3.
(32) Bocarsly, M.; Uzan, M.; Roy, I.; Grover, S.; Xiao, J.; Dong, Z.; Labendik, M.; Uri, A.; Huber, M. E.; Myasoedov, Y.; Watanabe, K.; Taniguchi, T.; Yan, B.; Levitov, L. S.; Zeldov, E. De Haas-van Alphen Spectroscopy and Magnetic Breakdown in Moiré Graphene. *Science* **2024**, *383* (6678), 42−48.
(33) Zhou, H.; Auerbach, N.; Uzan, M.; Zhou, Y.; Banu, N.; Zhi, W.; Huber, M. E.; Watanabe, K.; Taniguchi, T.; Myasoedov, Y.; Yan, B.; Zeldov, E. Imaging Quantum Oscillations and Millitesla Pseudomagnetic Fields in Graphene. *Nature* **2023**, *624* (7991), 275−281.
(34) Finkler, A.; Segev, Y.; Myasoedov, Y.; Rappaport, M. L.; Ne'eman, L.; Vasyukov, D.; Zeldov, E.; Huber, M. E.; Martin, J.; Yacoby, A. Self-Aligned Nanoscale SQUID on a Tip. *Nano Lett.* **2010**, *10* (3), 1046−1049.
(35) Finkler, A.; Vasyukov, D.; Segev, Y.; Ne'eman, L.; Lachman, E. O.; Rappaport, M. L.; Myasoedov, Y.; Zeldov, E.; Huber, M. E. Scanning Superconducting Quantum Interference Device on a Tip for Magnetic Imaging of Nanoscale Phenomena. *Rev. Sci. Instrum.* **2012**, *83* (7), 073702.
(36) Vasyukov, D.; Anahory, Y.; Embon, L.; Halbertal, D.; Cuppens, J.; Neeman, L.; Finkler, A.; Segev, Y.; Myasoedov, Y.; Rappaport, M. L.; Huber, M. E.; Zeldov, E. A Scanning Superconducting Quantum Interference Device with Single Electron Spin Sensitivity. *Nat. Nanotechnol.* **2013**, *8* (9), 639−644.
(37) Wyss, M.; Bagani, K.; Jetter, D.; Marchiori, E.; Vervelaki, A.; Gross, B.; Ridderbos, J.; Gliga, S.; Schönenberger, C.; Poggio, M. Magnetic, Thermal, and Topographic Imaging with a Nanometer-Scale SQUID-On-Lever Scanning Probe. *Phys. Rev. Appl.* **2022**, *17* (3). DOI: 10.1103/PhysRevApplied.17.034002.
(38) Vervelaki, A.; Bagani, K.; Jetter, D.; Doan, M.-H.; Chau, T. K.; Gross, B.; Christensen, D. V.; Bøggild, P.; Poggio, M. Visualizing Thickness-Dependent Magnetic Textures in Few-Layer $Cr_2Ge_2Te_6$. *Commun. Mater.* **2024**, *5* (1). DOI: 10.1038/s43246-024-00477-5.
(39) Aldeghi, M.; Allenspach, R.; Vervelaki, A.; Jetter, D.; Bagani, K.; Braakman, F.; Poggio, M.; Salis, G. Simulation and Measurement of Stray Fields for the Manipulation of Spin Qubits in One- and Two-Dimensional Arrays. *Nano Lett.* **2025**, *25* (5), 1838−1844.
(40) Weber, T.; Jetter, D.; Ullmann, J.; Koch, S. A.; Pfander, S. F.; Kress, K.; Vervelaki, A.; Gross, B.; Kieler, O.; Drechsler, U.; Baral, P. R.; Magrez, A.; Kleiner, R.; Knoll, A. W.; Poggio, M.; Koelle, D. Advanced SQUID-on-Lever Scanning Probe for High-Sensitivity Magnetic Microscopy with Sub-100-Nm Spatial Resolution. *Phys. Rev. Appl.* **2025**, *24*. DOI: 10.1103/6s24-vz3k.
(41) Akiyama, T.; De Rooij, N. F.; Staufer, U.; Detterbeck, M.; Braendlin, D.; Waldmeier, S.; Scheidiger, M. Implementation and Characterization of a Quartz Tuning Fork Based Probe Consisted of Discrete Resonators for Dynamic Mode Atomic Force Microscopy. *Rev. Sci. Instrum.* **2010**, *81* (6). DOI: 10.1063/1.3455219.
(42) Kort-Kamp, W. J. M.; Murdick, R. A.; Htoon, H.; Jones, A. C. Utilization of Coupled Eigenmodes in Akiyama Atomic Force Microscopy Probes for Bimodal Multifrequency Sensing. *Nanotechnology* **2022**, *33* (45), 455501.
(43) García, R. Dynamic Atomic Force Microscopy Methods. *Surf. Sci. Rep.* **2002**, *47* (6−8), 197−301.
(44) Troeman, A. G. P.; Van Der Ploeg, S. H. W.; Il'Ichev, E.; Meyer, H.-G.; Golubov, A. A.; Kupriyanov, M. Yu.; Hilgenkamp, H. Temperature Dependence Measurements of the Supercurrent-Phase Relationship in Niobium Nanobridges. *Phys. Rev. B* **2008**, *77* (2), 024509.
(45) Golubov, A. A.; Kupriyanov, M. Yu.; Il'ichev, E. The Current-Phase Relation in Josephson Junctions. *Rev. Mod. Phys.* **2004**, *76* (2), 411−469.
(46) Wölbing, R.; Schwarz, T.; Müller, B.; Nagel, J.; Kemmler, M.; Kleiner, R.; Koelle, D. Optimizing the Spin Sensitivity of Grain Boundary Junction nanoSQUIDs - towards Detection of Small Spin Systems with Single-Spin Resolution. *Supercond. Sci. Technol.* **2014**, *27*, 125007.
(47) Martínez-Pérez, M. J.; Koelle, D. NanoSQUIDs: Basics and Recent Advances. *Phys. Sci. Rev.* **2017**, *2* (8). DOI: 10.1515/psr-2017-5001.
(48) van Doorn, J. C. B. *Measuring the Current-Phase Relation of a Josephson Junction*; Leiden University, 2023.
(49) Regter, R. Q. *Towards Direct SQUID Readout of a Meissner Levitated Particle*; Leiden University, 2025.
(50) Persky, E.; Vardi, N.; Shperber, Y.; Kalisky, B. Improving the Sensitivity of Scanning Probe Microscopy with Mechanical Vibrations. *Appl. Phys. Lett.* **2018**, *113* (17). DOI: 10.1063/1.5051620.
(51) Tetienne, J.-P.; Dontschuk, N.; Broadway, D. A.; Stacey, A.; Simpson, D. A.; Hollenberg, L. C. L. Quantum Imaging of Current Flow in Graphene. *Sci. Adv.* **2017**, *3* (4). DOI: 10.1126/sciadv.1602429.
(52) Shibata, Y.; Nomura, S.; Kashiwaya, H.; Kashiwaya, S.; Ishiguro, R.; Takayanagi, H. Imaging of Current Density Distributions with a Nb Weak-Link Scanning Nano-SQUID Microscope. *Sci. Rep.* **2015**, *5* (1). DOI: 10.1038/srep15097.
(53) Huxter, W. S.; Palm, M. L.; Davis, M. L.; Welter, P.; Lambert, C.-H.; Trassin, M.; Degen, C. L. Scanning Gradiometry with a Single Spin Quantum Magnetometer. *Nat. Commun.* **2022**, *13* (1), 3761.
(54) Kuit, K. H.; Kirtley, J. R.; Van Der Veur, W.; Molenaar, C. G.; Roesthuis, F. J. G.; Troeman, A. G. P.; Clem, J. R.; Hilgenkamp, H.; Rogalla, H.; Flokstra, J. Vortex Trapping and Expulsion in Thin-Film $YBa_2Cu_3O_{7-\delta}$ Strips. *Phys. Rev. B* **2008**, *77* (13). DOI: 10.1103/PhysRevB.77.134504.

https://doi.org/10.1021/acs.nanolett.5c04571
Nano Lett. 2026, 26, 1608−1615